

Noninvasive Quantitation of Cerebral Blood Flow Using Oxygen-15-Water and a Dual-PET System

Hidehiro Iida, Shuichi Miura, Yasuaki Shoji, Toshihide Ogawa, Hirotsugu Kado, Yuichiro Narita, Jun Hatazawa, Stefan Eberl, Iwao Kanno and Kazuo Uemura

Department of Radiology and Nuclear Medicine, Research Institute for Brain and Blood Vessels, Akita, Japan

Measurement of the arterial input function is essential for quantitative assessment of physiological function in vivo using PET. However, frequent arterial blood sampling is invasive and labor intensive. Recently, a PET system has been developed that consists of two independent PET tomographs for simultaneously scanning the brain and heart, which should avoid the need for arterial blood sampling. The aim of this study was to validate noninvasive quantitation with this system for ^{15}O -labeled compounds. **Methods:** Twelve healthy volunteers underwent a series of PET studies after C^{15}O inhalation and intravenous H_2^{15}O administration using a Headtome-V-Dual tomograph (Shimadzu Corp., Kyoto, Japan). The C^{15}O study provided gated blood-pool images of the heart simultaneously with quantitative static blood-volume images of both the brain and heart. Weighted-integrated H_2^{15}O sinograms were acquired for estimating rate constant (K_1) and distribution-volume (V_d) images in the brain, in addition to single-frame sinograms for estimating autoradiographic cerebral blood flow images. Noninvasive arterial input functions were determined from the heart scanner (left ventricular chamber) according to a previously developed model and compared directly to invasive input functions measured with an on-line beta probe in six subjects. **Results:** The noninvasive input functions derived from this PET system were in good agreement with those obtained by continuous arterial blood sampling in all six subjects. There was good agreement between quantitative values obtained noninvasively and those using the invasive input function: average autoradiographic regional cerebral blood flow was 0.412 ± 0.058 and 0.426 ± 0.062 ml/min/g, K_1 of H_2^{15}O was 0.416 ± 0.073 and 0.420 ± 0.067 ml/min/ml and V_d of H_2^{15}O was 0.800 ± 0.080 and 0.830 ± 0.070 ml/ml for the noninvasive and invasive input functions, respectively. In addition to the brain functional parameters, the system also simultaneously provided cardiac function such as regional myocardial blood flow (0.84 ± 0.19 ml/min/g), left ventricular volume (132 ± 22 mm at end diastole and 45 ± 14 ml at end systole) and ejection fraction ($66\% \pm 5\%$). **Conclusion:** This PET system allows noninvasive quantitation in both the brain and heart simultaneously without arterial cannulation, and may prove useful in clinical research.

Key Words: PET; cerebral blood flow; arterial input function; noninvasive quantitation; myocardial blood flow

J Nucl Med 1998; 39:1789-1798

Determination of the arterial input function is essential for quantitating physiological function in vivo using PET. The arterial input function is usually measured by frequent or continuous arterial blood sampling from a peripheral artery such as the radial artery. This procedure is both laborious and invasive and may be a source of additional errors in the parameter estimates, because even small distortions in the measured input function can cause significant errors in the calculated physiological parameters (1,2). Accurate corrections for delay and dispersion in the ob-

served arterial time-activity curve seem to be particularly critical in studies with ^{15}O -labeled compounds.

There has been considerable effort to replace arterial cannulation in quantitative PET studies with less invasive methods. Standardized input functions calibrated by a minimal number of arterial or venous blood samples are being used for clinical studies. However, the standardized input function method has only been validated for tracers with slow kinetics, such as ^{18}F -labeled fluorodeoxyglucose (3,4) and ^{123}I -labeled iodoamphetamine in SPECT (5-7). The standardized input function technique is unlikely to be applicable to tracers with rapid kinetics such as ^{15}O -labeled compounds. For these tracers, calculated physiological parameters are highly sensitive to small distortions of the input function, resulting in large errors in the calculated parameters for even small differences between of the shape of the individual and standardized input functions (1,2,8,9).

Previous studies have attempted to noninvasively measure the individual input function after intravenous ^{15}O -water (H_2^{15}O) administration with external detectors. Of these, scanning the wrist (the radial and/or ulnar artery) with a small PET scanner provided significant signal with only a small amount of spillover from the soft tissue. However, the small recovery coefficient (<0.1) largely prevented accurate absolute quantitation (9). Additionally, the dispersion was found to be too large in the radial artery system due to a long transit time, unless the arterial blood is withdrawn by a pump. Scanning the neck (the carotid artery) (10), which may be performed by extending the axial field of view of the PET scanner, demonstrated significant signal in the carotid artery. However, the heterogeneous structures surrounding the carotid artery made the required model-based correction for the non-negligible amount of spillover from the soft tissue difficult. Again, accurate correction for the small recovery coefficient (≈ 0.1) was not possible.

Other investigators have applied a mathematical model, in which the arterial input function was estimated directly from the dynamic PET tissue images (11-13). Although theoretically valid, in practice several sources of error prevented stable results to be obtained for the estimated parameters. These methods provided images that correlated well with the functional images but failed to provide absolute quantification (13).

It has been shown that the arterial input function after H_2^{15}O administration can be accurately estimated from the dynamic images in myocardial PET studies, enabling quantification of regional myocardial blood flow (MBF) without arterial blood sampling (14-17). Good counting statistics, which have been shown to be important for minimizing the systematic bias and statistical uncertainty of the estimated parameters, were obtained by defining a moderately large region of interest (ROI) inside the left ventricular chamber. Corrections for the recovery coefficient of the left ventricular (or the left atrial) chamber (≈ 0.8) and the spillover from the myocardial radioactivity could be performed using a mathematical model previously validated in greyhound experiments (14). Thus, an independent

Received Jun. 18, 1997; revision accepted Jan. 26, 1998.

For correspondence or reprints contact: Hidehiro Iida, DSc, Department of Radiology and Nuclear Medicine, Research Institute for Brain and Blood Vessels, 6-10 Senshu-Kubota-Machi, Akita City, Akita 010 Japan.

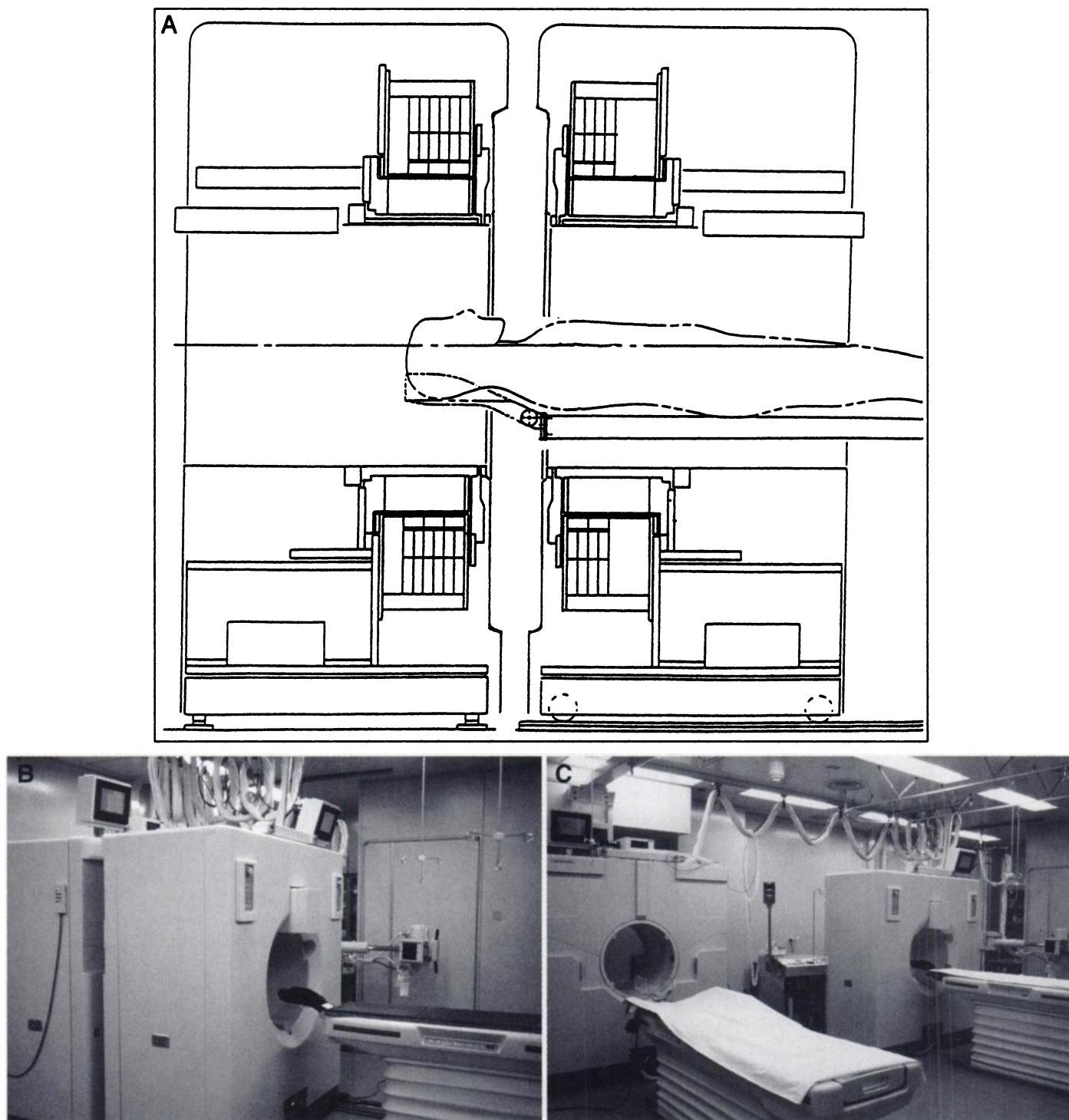


FIGURE 1. (A) Cross-sectional view of Headtome-V-Dual scanner. (B) Use as dual-PET scanner. (C) Use as two independent scanners.

PET scanner centered over the heart could be used to accurately determine the input function noninvasively in quantitative neurological PET studies. Based on this, we have developed a new PET system, Headtome-V-Dual (Shimadzu Corp., Kyoto, Japan) that essentially consists of two independent PET tomographs. The two PET systems can be configured for the whole brain and heart to be scanned simultaneously (18). Thus, this system has the potential to provide noninvasive input functions for cerebral studies by monitoring the time-activity curves in the left ventricle. Furthermore, this scanner allows simultaneous assessment of physiological function in both the brain and the heart.

The aim of this study was to validate the accuracy of using

the left ventricular time-activity curve for noninvasive quantitation in clinical $H_2^{15}O$ studies. The previously proposed mathematical model (17) for spillover correction has only been validated in greyhounds that have larger left ventricular chambers and recovery coefficients than those expected in human studies. Thus, this study extends the model validation to human studies in a clinically practical setting.

MATERIALS AND METHODS

Scanner Design

The system consists of two independent PET tomographs as shown in Figures 1A and B. The brain scanner can move perpen-

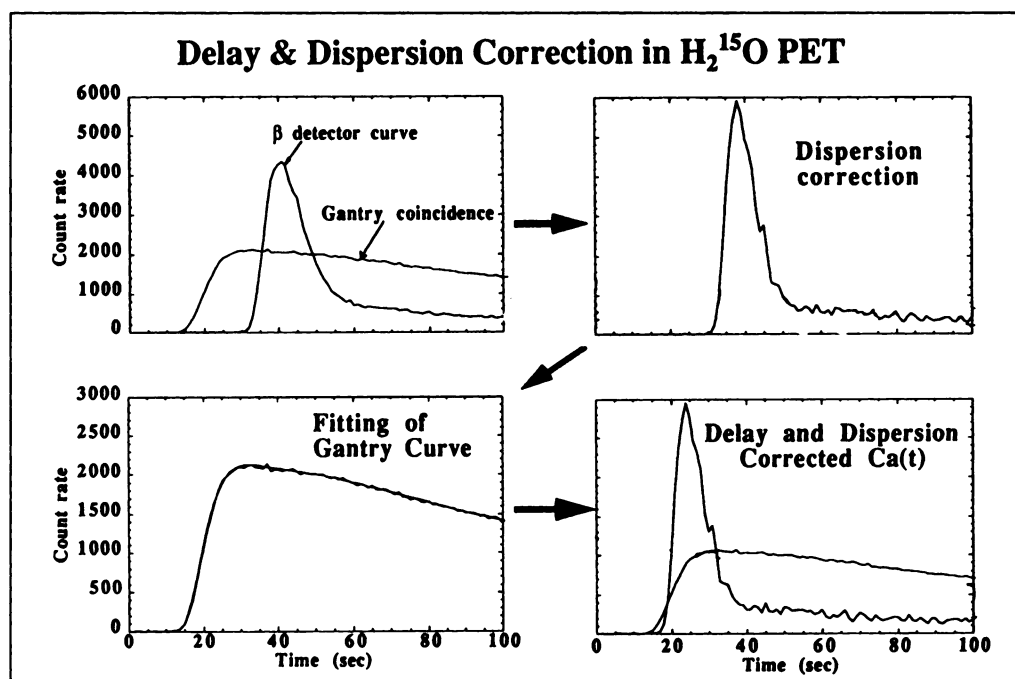


FIGURE 2. Procedure of delay and dispersion correction. Upper left: Observed beta detector curve and total coincidence curve of midbrain slice. It can be seen that the beta-probe curve is significantly delayed compared with whole-brain coincidence curve because of longer transit time in peripheral arterial system. Upper right: Arterial curve corrected for dispersion by deconvolving beta-probe curve by single exponential function with fixed dispersion time constant ($\tau = 4$ sec), which corresponds to relative dispersion of beta-probe curve compared with true input function for brain. Lower left: Delay adjustment by fitting detector coincidence curve to simulated, single compartment model, whole brain tissue curve. Three parameters (delay, K_1 , and k_2) were fitted to first 60 sec of data by nonlinear least-squares optimization. Lower right: Dispersion and delay corrected input function and whole-detector brain coincidence curve.

dicular to the bed axis, allowing it to be used separately as two independent tomographs (Fig. 1C). Data can be acquired in each scanner independently and are transferred to a conventional workstation (TITAN 2; Kubota, Tokyo, Japan) for further manipulations. Each scanner can be controlled separately from either of the two consoles (independent operation of the two scanners) or one of the two workstations can operate both scanners through the network (combined scanner operation). Axial movement of the heart gantry allows adjustment of the distance between brain and heart in each study. The axial fields of view are 15 and 10 cm for the brain and heart scanners, respectively. The distance from the gantry surface to the first detector ring is 58 mm, leaving a gap between the two gantries of approximately 15–20 cm in typical studies. This allows subjects to place their arms between the two gantries, facilitating intravenous administration into one of the arms. The minimum distance between the heart and brain fields of view is approximately 130 mm. Each gantry consisted of 850-mm rings containing 112 U two-dimensional position-sensitive detector blocks each. Three rings were used in the brain gantry and two rings in the heart gantry. The septa can be retracted in each scanner for three-dimensional data acquisition. The physical geometry and its basic performance have been described previously (18).

The axial coincidence path acceptance was optimized in the two-dimensional acquisition mode to maximize the peak noise-equivalent counting rate (NEC), resulting in use of 5 slice pairs for the direct and 6 slice pairs for the cross planes (18). For the brain scanner, slices were rebinned by adding sinograms in groups of two with a 1-slice overlap between adjacent groups, resulting in 46 reconstructed slices at 3.125-mm intervals. For the heart scanner, groups of four sinograms were added, again with a 1-slice overlap, to yield 10 reconstructed slices spaced 9.375 mm apart. The rebinning resulted in effective sensitivities per tomographic slice of 10 kcps/ml/ μ Ci for the brain and 20 kcps/ml/ μ Ci for the heart. The scanner is capable of simultaneously acquiring dynamic or gated data with static data and can also perform on-line weighted-integration frame collection simultaneously with the conventional static or dynamic scans.

Subjects

The study population consisted of 12 healthy volunteers (10 men, 2 women; aged 22–69 yr; mean \pm s.d. 41 ± 18) (Table 1).

All subjects underwent brain MRI scans (T1- and T2-weighted images) on the same day as the PET scan. A medical review excluded past history of cardiac or cerebrovascular disease, and tests showed no evidence of diabetes mellitus, hypertension or elevated cholesterol levels in any of the subjects. The laboratory tests also included a screen for serum electrolytes (sodium, potassium, chlorine), creatinine and blood urea nitrogen, fasting blood glucose, triglyceride, uric acid and total plasma protein. Seven of the volunteers were nonsmokers and five were smokers. All volunteers gave written informed consent to the protocol approved by the Ethics Committee of Research Institute for Brain and Blood Vessels, Akita, Japan.

PET Protocol

A catheter was placed in the antecubital vein for administration of $H_2^{15}O$ and for blood sampling during the $C^{15}O$ scan. In the first six subjects (Table 1), an arterial cannula was also placed in the radial artery, and arterial blood radioactivity concentration was continuously monitored during the $H_2^{15}O$ scan using a beta probe (8) to directly validate the noninvasive input function.

Subjects were in the supine position on the scanner bed with their arms placed between the two gantries. After positioning the head on the scanner bed, the heart gantry was positioned with a help of an on-line display of projection images from $C^{15}O$ gas inhaled for 1 min (approximately 5 GBq supplied to mouth of the subject). Positioning of the heart gantry typically required less than 1 min. A tomographic, gated-blood-pool scan was started on the heart scanner 1 min after the end of inhalation. This scan lasted for approximately 6 min (≈ 400 beats). The gate sequence was triggered by the R-wave on the electrocardiogram. At 4 min after the start of the $C^{15}O$ inhalation, a 4-min static scan was acquired on both the brain and the heart scanners (i.e., simultaneous gated and static scans on the heart scanner). During the static scan, three blood samples were taken from the antecubital vein and counted in a well counter cross calibrated to the PET scanner to quantitate blood volume. The recovery coefficient of the left ventricular chamber was also obtained from the static blood-volume image of the heart.

After the $C^{15}O$ scan, 10-min transmission scans were obtained using rotating rod sources (≈ 300 MBq ^{68}Ge) in both scanners simultaneously. Immediately after the transmission scans, $H_2^{15}O$

TABLE 1
Subject Data

Subject no.	Age (yr)	Sex	Weight (kg)	HR (min ⁻¹)	Systolic blood pressure (mm Hg)	RPP	PaCO ₂ (mm Hg)	Hct (%)	Hb (g/100 ml)
1	48	M	65	79	118	9322	42.6	45.5	14.2
2	59	M	73	58	114	6612	39	39	13.1
3	69	M	49	66	120	7920	39	39	11.6
4	65	F	52	57	138	7866	42.5	42.5	10.4
5	51	M	67	58	148	8584	43.8	43.8	12.7
6	51	F	50	56	104	5824	39.1	39.1	10.3
7	25	M	65	76	105	7980	40	41.5	13.6
8	26	M	73	61	116	7076	41	49.5	14.9
9	24	M	65	55	92	5060	39	43	13.5
10	22	M	60	58	99	5742	42	43.5	14
11	24	M	57.5	57	90	5130	46.7	46	14.5
12	23	M	56	59	101	5959	40	46	14.1
Mean ± s.d.	41 ± 18		61 ± 9	62 ± 8	112 ± 18	6923 ± 1409	41 ± 2	43 ± 3	13.1 ± 1.5

*Invasive arterial input function was measured in the first six subjects to validate the noninvasive input function.

HR = heart rate; RPP = rate-pressure product; Hct = hematocrit; Hb = hemoglobin.

was infused continuously into the antecubital vein for 2 min, and scans commenced on both the brain and heart scanners at the start of H₂¹⁵O infusion. The brain scanner acquired two weighted-integrated sinograms with weight functions of unity and time (19, 20) and an integration time of 6 min. A single, static frame was also acquired simultaneously during the first 3 min. At the same time, the heart scanner acquired the following dynamic frames: 6 × 5 sec, 6 × 15 sec and 8 × 30 sec, for a total 20 frames over 6 min.

In six subjects, arterial blood was continuously withdrawn during the H₂¹⁵O study at a rate of 5 ml/min, and its radioactivity concentration was monitored using a beta probe (8). The tube was approximately 20-cm long and the inner diameter was 0.5 mm. Dispersion and the delay in the tube was negligibly small (8). Using a tube filled with radioactive water, the beta probe was cross calibrated to the well counter, which in turn was cross calibrated to the PET scanner.

Arterial (Invasive) Input Function

Figure 2 illustrates the procedure for obtaining the input function from the arterial time-activity curve. First, the observed beta-probe curve was corrected for decay and calibrated to the two PET scanners through the well counter. The curve was then corrected for dispersion in the radial artery by deconvolving it with a single exponential function, assuming a fixed dispersion time constant of 4 sec (7). The curve was also corrected for delay (i.e., longer transit time to the radial artery compared to that to the brain) by fitting the whole-brain tissue time-activity curve (gantry coincidence curve of the brain scanner) to a single-tissue compartment model. The influx (K₁) and outflux (k₂) rate constants and the delay (Δt) were optimized with nonlinear least-square fitting to the total coincidence curve from the midbrain slice (2).

Noninvasive Input Function

The noninvasive input function was calculated from the left ventricular time-activity curve as previously reported (14). This procedure included corrections for the limited recovery of the left ventricular ROI and spillover from the tissue into the left ventricular ROI. Two ROIs were placed, one to cover the whole left ventricular chamber and another to cover the whole myocardial wall on the midventricular tomographic slice, as shown in Figure 3. The left ventricular chamber and myocardial time-activity curves from these two ROIs were then fitted to the model equations as follows:

$$LV(t) = \beta \cdot C_a(t) + (1 - \beta) \cdot C_t(t), \quad \text{Eq. 1}$$

$$R(t) = \alpha \cdot C_t(t) + V_a \cdot C_a(t) \quad \text{Eq. 2}$$

and

$$C_t(t) = f \cdot C_a(t) \otimes e^{-f/p \cdot t}, \quad \text{Eq. 3}$$

where \otimes denotes the correlation integral, LV(t) (Bq/ml) and R(t) (Bq/ml) represent the time-activity curves in the left ventricular chamber and myocardial ROIs, respectively, C_a(t) (Bq/ml) the true input function, free from the limited recovery and spillover, C_t(t) (Bq/g) the true myocardial time-activity curve, β the recovery coefficient of the left ventricular chamber, α (g/ml) the recovery coefficient of the myocardial ROI (fraction of water-perfusible tissue within the ROI), f (ml/min/g) the regional MBF, p (ml/g) the tissue-to-blood partition coefficient (assumed to be 0.91 ml/g) and V_a (ml/ml) the spillover of the blood activity into the myocardial ROI. The recovery coefficient, β, was determined from the C¹⁵O scan by dividing the radioactivity concentration in the left ventricular ROI (Bq/ml) by the blood activity measured in the cross calibrated well counter (Bq/g) and then dividing by the blood density [1.06 (g/ml)]. Kinetic fitting of LV(t) and R(t) curves to the above equations, using the fixed β value from the C¹⁵O scan, provided the parameters f, α and V_a, and thus yielded the true input function as:

$$C_a(t) = \frac{1}{\beta} \cdot LV(t) - \frac{(1 - \beta)}{\beta^2} \cdot f \cdot LV(t) \otimes e^{-\{1/p + (1 - \beta)/\beta\} \cdot f \cdot t}. \quad \text{Eq. 4}$$

Before application to the brain data, the generated input curve was corrected for delay in the same way as the invasive input function, i.e., the three parameters of influx (K₁) and outflux (k₂) rate constants and the delay (Δt) were fitted to the total coincidence curve from the midbrain slice. The fitted delay was considered to be the mean transit time from the heart to the brain. No correction was made for dispersion in the noninvasive input function, because of the short transit time (1–4 sec as measured in this study) from the heart to the brain.

Functional Image Calculation

All images were reconstructed using filtered backprojection. Regional cerebral blood flow (CBF) images were calculated with the H₂¹⁵O autoradiography method (21,22) using the data acquired for the first 3 min after the H₂¹⁵O administration. Functional parametric images of K₁ and V_a of H₂¹⁵O were also calculated for the brain using the two weighted-integrated images (19,20).

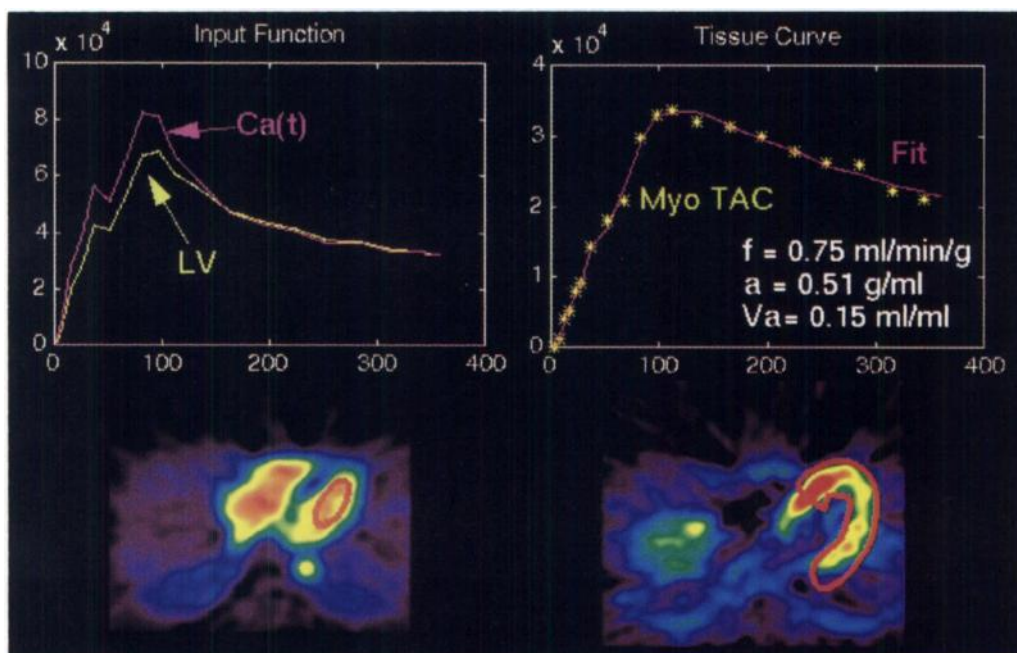


FIGURE 3. Generation of noninvasive input function from dynamic H_2^{15}O images of heart. Two ROIs were drawn: one on left ventricular chamber on C^{15}O image (bottom left) and the other on myocardial region on MBF image (bottom right). Three parameters: regional MBF, recovery coefficient of myocardium and spillover from blood into myocardial region, were fitted to model equations described in text. LV (top left) corresponds to left ventricular time-activity curve, and Myo TAC (asterisks on top right) corresponds to measured myocardial regional time-activity data. Fit denotes fitted time-activity curve and $\text{Ca}(t)$ is estimated true input function.

Functional images were calculated with both the invasive and noninvasive input functions.

Regions-of-Interest Analysis

CBF images were registered to the corresponding MR images in each study using a fully automated method (23). A total of 39, circular ROIs were defined on the MR images of each subject over both hemispheres according to the criteria of Yamaguchi et al. (24) as shown in Table 2. Relatively large ROIs with diameters of 20 mm were drawn to minimize the effects of anatomical uncertainty and to decrease intersubject variability.

Cardiac Blood-Pool Volume Estimation

Volume of the left ventricular chamber was measured using the gated blood-pool images of the heart. The border of the left ventricular chamber was manually defined by tracing at the 70% count level around the left ventricular blood-pool images on both the end-diastolic and end-systolic images, and the ejection fraction (EF) was calculated from these two volumes.

Statistical Analysis

All data are presented as mean \pm s.d. Paired data were compared with the paired Student's *t*-test, and Bonferroni correction was applied where appropriate. A *p* value < 0.05 was considered to be statistically significant.

RESULTS

The coincidence counting rates of the middle slice of the brain and heart scanners after the infusion of H_2^{15}O are shown in Figure 4 for a typical study. The peak totals (i.e., trues and randoms) and random counting rates for the middle slice were 3–5 kcps and 1–2 kcps for the brain scanner and 15–20 kcps and 6–9 kcps for the heart scanner, respectively. The peak counting rates for all the slices were typically 40–50 kcps (totals) and 15–25 (randoms) and 50–70 kcps (totals) and 25–35 (randoms) for the brain and heart scanners, respectively. The NEC as defined by Strother et al. (25) was then estimated as approximately 23–25 kcps and 25–35 kcps for the brain and heart scanners, respectively. The deadtime correction factor was < 2.0 throughout the scan period in both scanners.

Figure 5 compares a typical noninvasive input function obtained from the left ventricular time-activity curve with the invasive input function from continuous arterial blood sampling. Agreement between the two input functions was visually confirmed in all six studies. Figure 6 compares typical functional images of CBF (H_2^{15}O autoradiography) calculated with the noninvasive input function with those obtained with the invasive input function. Figure 7 plots autoradiographic CBF, K_1 and V_d of water in cortical gray matter calculated with the noninvasive input function and with the invasive input function. There was no significant difference in the calculated parameters between the two input function methods. Quantitative CBF values obtained by the dual-PET system, as well as those by the invasive input function are summarized in Table 2. Statistical analysis showed no significant difference in the calculated CBF values between the two input functions in any of the regions.

Other quantitative results using the noninvasive method are summarized in Table 3. The cerebral blood volume was obtained from the C^{15}O scan in the brain. The end-systolic and end-diastolic volumes of the left ventricular chamber and the EF were estimated from the C^{15}O scan in the heart (Fig. 8). Regional MBF averaged over the whole myocardial wall, perfusable-tissue index, perfusable tissue fraction and the heart-to-brain transit time were obtained from the ^{15}O -water scan.

A significant correlation was observed between the average MBF and the systolic blood pressure (SBP); $\text{MBF} = -0.176 + 0.00934 \times \text{SBP}$ ($r = 0.82$, $p < 0.001$). A significant correlation was also observed between MBF and the heart rate and systolic blood pressure product (RPP); $\text{MBF} = 0.036 + 0.0001206 \times \text{RPP}$ ($r = 0.85$, $p < 0.001$).

DISCUSSION

This study demonstrates that the arterial input function, i.e., the whole-blood radioactivity concentration curve after intravenous H_2^{15}O administration, can be accurately determined without arterial blood sampling. Limited recovery of the left ventricular chamber (≈ 0.8) and spillover from the myocardial signal into the left ventricular chamber were successfully

TABLE 2
Summary of Cerebral Blood Flow Values Calculated by Oxygen-15-Water Autoradiography

Regions	Cerebral blood flow (ml/min/100 g)		
	Noninvasive by dual-PET (n = 12)	Noninvasive by dual-PET (n = 6)	Invasive by arterial sampling (n = 6)
Brain stem			
Pons	36.6 ± 8.5	40.3 ± 6.4	39.9 ± 5.9
Midbrain	36.4 ± 8.8	39.0 ± 5.4	38.7 ± 5.8
Cerebellum			
Vermis	42.9 ± 7.9	42.3 ± 4.2	41.7 ± 3.6
Right hemisphere	43.4 ± 11.1	42.6 ± 5.0	41.8 ± 4.3
Left hemisphere	47.2 ± 12.2	45.8 ± 7.2	45.2 ± 6.2
Caudate			
Right	41.9 ± 11.3	44.4 ± 8.2	44.5 ± 8.4
Left	41.6 ± 7.1	44.9 ± 7.3	46.1 ± 10.0
Lentiform			
Right	47.0 ± 9.2	50.0 ± 7.0	51.1 ± 7.2
Left	45.7 ± 8.6	47.2 ± 5.8	46.7 ± 4.7
Thalamus			
Right	47.1 ± 11.4	46.8 ± 7.7	46.5 ± 7.0
Left	42.1 ± 10.5	47.3 ± 9.5	46.9 ± 8.7
Temporal			
Right			
Hippocampus	35.9 ± 10.1	39.9 ± 9.6	38.7 ± 8.7
Sup temp gy	48.9 ± 9.9	48.0 ± 6.9	48.0 ± 5.6
Mid temp gy	41.6 ± 8.9	42.2 ± 9.4	41.6 ± 8.2
Inf temp gy	35.3 ± 6.7	37.9 ± 6.4	36.8 ± 6.1
Left			
Hippocampus	33.2 ± 9.7	38.5 ± 6.9	37.6 ± 6.5
Sup temp gy	46.2 ± 7.9	49.7 ± 8.0	49.6 ± 6.7
Mid temp gy	40.6 ± 10.2	42.3 ± 11.8	41.0 ± 11.0
Inf temp gy	34.6 ± 7.9	34.7 ± 7.0	33.2 ± 6.2
Frontal			
Right			
Cingulate	38.2 ± 10.4	43.7 ± 7.6	43.3 ± 7.0
Sup fro gy	38.2 ± 11.4	43.0 ± 11.8	42.2 ± 10.9
Mid fro gy	33.5 ± 8.9	36.4 ± 6.7	35.4 ± 6.3
Inf fro gy	38.0 ± 9.6	39.4 ± 7.3	38.2 ± 6.4
Precentral	41.3 ± 7.5	41.3 ± 4.3	40.6 ± 3.9
Left			
Cingulate	35.3 ± 8.9	41.0 ± 6.4	41.2 ± 6.5
Sup fro gy	36.9 ± 7.6	38.9 ± 5.7	38.3 ± 5.2
Mid fro gy	33.4 ± 8.1	36.5 ± 5.4	35.8 ± 5.0
Inf fro gy	39.7 ± 10.6	39.7 ± 3.9	39.2 ± 3.3
Precentral	38.5 ± 6.7	39.1 ± 3.0	38.2 ± 2.4
Parietal			
Right postcentral	37.9 ± 5.9	39.6 ± 4.4	38.9 ± 4.2
Left postcentral	38.4 ± 8.1	40.7 ± 7.6	39.7 ± 8.0
Occipital			
Right			
Cuneus	47.6 ± 8.7	46.6 ± 6.1	46.3 ± 5.4
Post occ area	41.3 ± 8.5	45.7 ± 7.2	45.3 ± 7.5
Lateral occ area	35.2 ± 7.2	38.5 ± 7.7	37.6 ± 7.6
Left			
Cuneus	47.4 ± 13.5	48.9 ± 16.1	47.3 ± 12.8
Post occ area	38.4 ± 10.6	42.4 ± 12.6	40.7 ± 9.6
Lateral occ area	30.3 ± 6.8	31.6 ± 6.0	30.4 ± 5.5
Semioval center			
Right	23.7 ± 3.7	25.4 ± 3.3	24.0 ± 2.3
Left	23.2 ± 4.9	24.3 ± 4.7	22.8 ± 4.9
Total average	39.1 ± 7.4	41.2 ± 5.8	40.5 ± 5.0
Cortical gray matter	39.4 ± 7.3	41.6 ± 6.1	40.9 ± 5.2
Deep gray matter	40.9 ± 8.0	42.8 ± 5.3	42.6 ± 5.1
White matter	23.5 ± 4.1	24.8 ± 3.6	23.4 ± 3.7
Cerebellum	39.9 ± 8.8	40.5 ± 5.2	39.7 ± 4.6

Sup = superior; temp = temporal; mid = middle; inf = inferior; fro = frontal; occ = occipital; gy = gyrus.

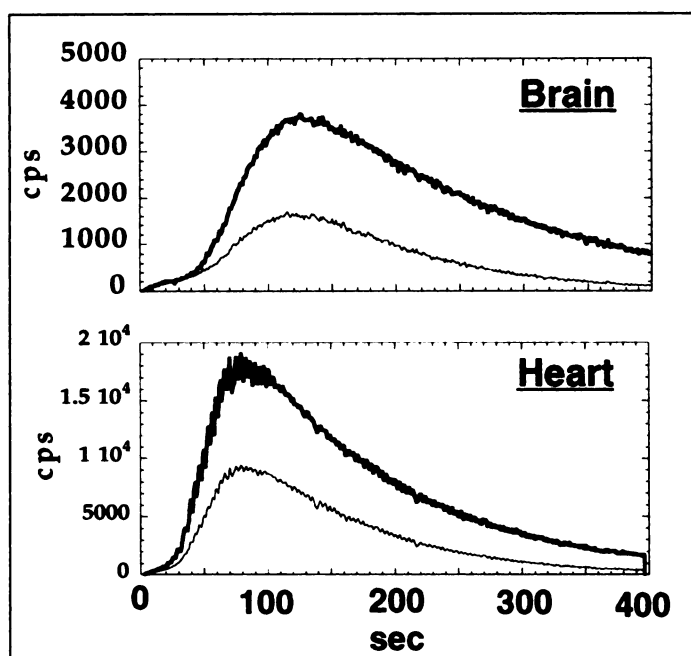


FIGURE 4. Total coincidence (bold lines) and random event (thin lines) counting rates at center slice of brain and heart scanners. Net coincidence event rates correspond to total – randoms. Note: higher than expected randoms rate at early time points (~ 0 –50 sec) is due to randoms from dose in injection line outside direct field of view of scanners.

corrected with a previously reported method (14). The good agreement between the estimated and directly measured input functions and the good agreement of the CBF values calculated with the two input functions confirms the previous greyhound validation. The quantitative MBF values in the healthy volunteers in this study were in a good agreement with our previous data, and significantly correlated with RPP as well as SBP, further validating the quantitative accuracy of the heart scanner.

The intersubject variation of regional CBF values of approximately $\pm 10\%$ – 15% is consistent with our previous data based

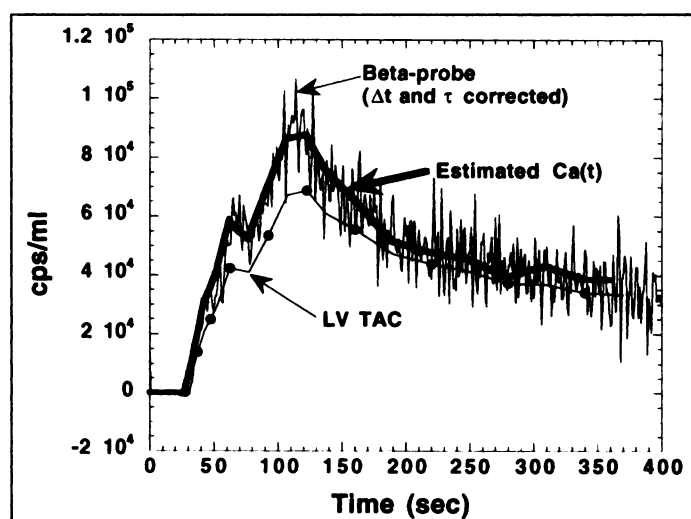


FIGURE 5. Comparison of noninvasive input function generated from left ventricular time-activity curve (LV TAC) with invasive input function from beta probe. Solid line with closed circles denotes LV TAC. Bold solid line denotes estimated noninvasive input function [estimated $\text{Ca}(t)$], and thin solid line corresponds to invasive input function obtained using beta detector. Both input functions have been corrected for delay and decay of H_2^{15}O . Dispersion has also been corrected for invasive input function but not for noninvasive input function. Small dip in rise of invasive input function, which was occasionally observed in this study, was also well reproduced with noninvasive input function.

on arterial blood sampling (24,26) and also validates the accuracy of the simultaneous measurement of the brain and the heart. The average CBF values obtained in this study also agreed well with the normal CBF values obtained previously in this laboratory using the steady-state technique (24) but are about 20% lower than our previous H_2^{15}O autoradiography normal values (26). This difference is attributed to different delay adjustment in the previous studies (26), in which the delay was determined by linear extrapolation of the rising slope of both the arterial and whole tissue curves (22), which was found to cause misadjustment of 4–6 sec, resulting in an overestimation of CBF by approximately 20% (2). The improved method of estimating delay by fitting to the total coincidence curve of the midbrain slice has been used in this article and accounts for the difference from previously published normal CBF values.

Use of the left ventricular time-activity curve for determining the input function eliminates the need for arterial cannulation, which has advantages in clinical studies. It avoids the risk of vasospasm and/or hemorrhage in the peripheral arterial line and largely removes the mental stress on the subject due to the arterial cannulation, which is particularly important for neurological studies. Furthermore, the amount of blood withdrawn is no longer a limiting factor for long data acquisition periods, and thus kinetic analysis can be performed for a long scanning period with full measurement of the input curve. Noninvasive sampling of the input curve is particularly advantageous when acquiring real-time weighted-integration data (19), because the scan period can be prolonged as long as required for the kinetic analysis, without limitations imposed by the blood sampling.

This study also demonstrates that the simultaneous quantitation in the brain and heart is valid. Although the counting rates in the heart scanner were higher than those in the brain scanner after H_2^{15}O administration, the deadtime correction factor was small enough throughout the study to maintain quantitative accuracy in both scanners. To reduce the deadtime correction factor and random rates in our protocol, an infusion over 2 min (rather than a bolus injection) was used.

Oxygen-15-labeled compounds are capable of measuring several fundamental physiological parameters in the myocardium, e.g., regional MBF (16,27), water perfusable tissue fraction (28–30), oxygen extraction fraction and oxygen metabolism (31,32). Simultaneous measurement of these functional parameters in both brain and heart may be of clinical interest, such as determination of the cerebral flow reserve in candidates for coronary artery surgery. However, the clinical use of this combined information is still unknown, and further investigations are needed.

The C^{15}O inhalation PET scan facilitated accurate positioning of the heart gantry. This was important, because the present system has an axial field of view for the heart scanner of only 10 cm and precise positioning was required. Although the heart gantry also could have been positioned with a transmission scan, the C^{15}O approach provides better positioning accuracy in a shorter time. The C^{15}O data were also used for defining left ventricular ROI and proved useful for evaluating myocardial wall motion, end-systolic and end-diastolic left ventricular volume and EF. The time period required for this scan was short, approximately 15 min. Inclusion of the C^{15}O scan is therefore not limiting for routine clinical studies and may prove clinically useful, particularly in patients with cardiac disease.

Determination of the input function from the heart scanner may be limited for other tracers such as receptor ligands, which often require determination of metabolites in the arterial blood that cannot be directly measured by scanning the vasculature. The arterial metabolites may, however, be predicted in certain

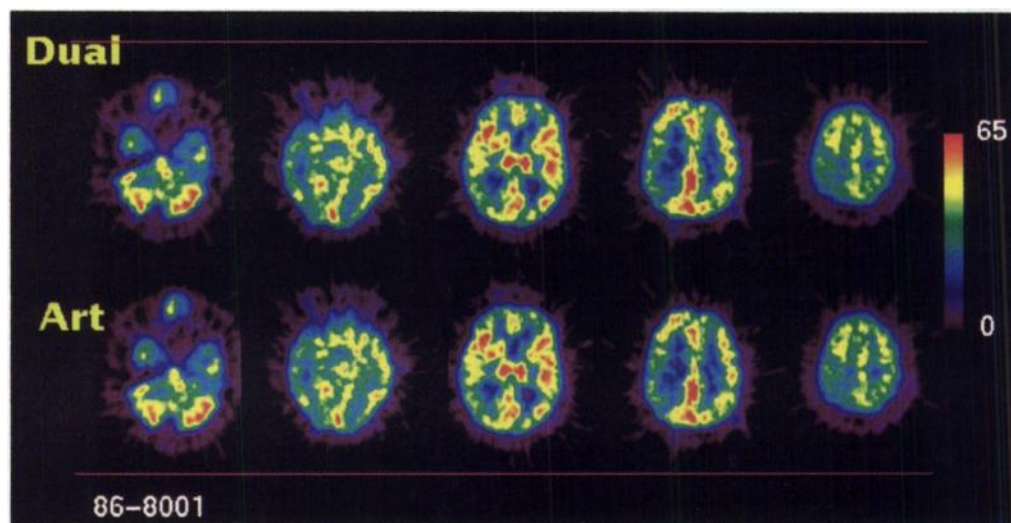


FIGURE 6. Comparison of CBF images calculated by H_2^{15}O autoradiography using noninvasive input function (Dual) with those using arterial blood sampling (Art). All images are displayed with same absolute color scale.

situations by modeling, as has been successfully done for H_2^{15}O inhalation studies. Iida et al. (33) demonstrated that the arterial metabolites (i.e., recirculating H_2^{15}O) can be accurately estimated from the whole-blood radioactivity concentration curve by assuming a constant rate of recirculating water production in the whole body. Further studies are, however, required to investigate the applicability of this technique to other tracers that demand metabolite corrections.

All software programs of the two gantries can be operated from either one of the UNIX workstations through the network, which enables use of several macroprocesses for the data acquisition and image analyses. This allows the quantitative parametric images to be generated easily and quickly immediately after the completion of the study.

The dual-PET system is particularly advantageous for studies with ^{15}O compounds. Inappropriate delay and dispersion correction of the arterial input curve has been one of the most important sources of errors in ^{15}O -labeled tracer studies. Because of a shorter transit time from the left ventricle to the brain than that from the left ventricle to the radial artery, the correction for delay and dispersion should be more accurate with the noninvasive method.

Eliminating the need for arterial cannulation with our dual-PET system should increase the throughput for quantitative clinical studies. The extended axial field of view of the two gantries combined should also decrease the scanning time for whole-body studies, further improving clinical throughput.

CONCLUSION

The dual-PET system has been validated for quantitative studies using intravenous H_2^{15}O and C^{15}O inhalation studies. This system allows noninvasive quantitation in both brain and heart simultaneously without arterial cannulation and may be of use in clinical research studies.

ACKNOWLEDGMENTS

We are indebted to the technical staff of the Department of Radiology and Nuclear Medicine, Research Institute for Brain and Blood Vessels, Akita, Japan for technical assistance. This work was supported in part by a research grant for cardiovascular diseases (8C-5, 1997) from the Ministry of Health and Welfare. This work was presented at the 43rd Annual Meeting of the Society of Nuclear Medicine, Denver, Colorado, 1996 (34).

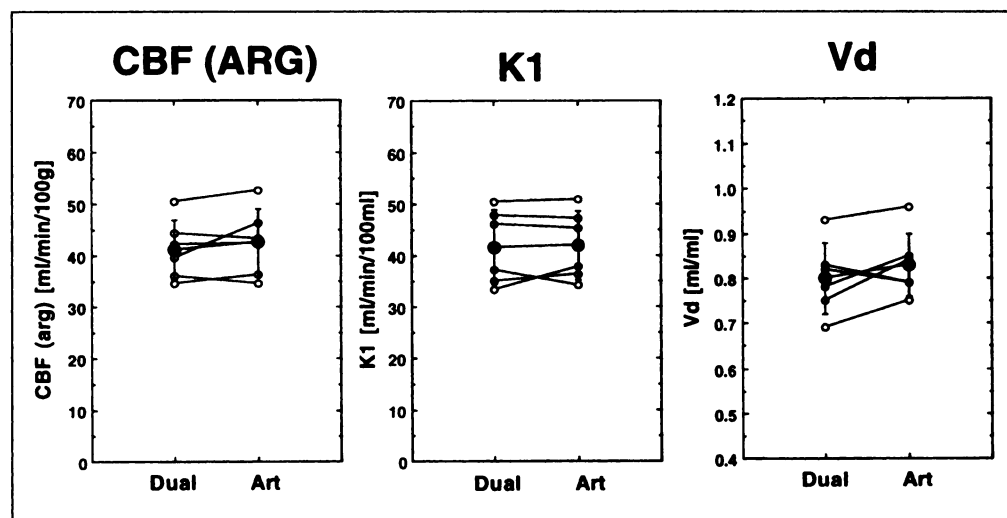


FIGURE 7. Comparison of quantitative parameters in brain obtained with noninvasive input function with those obtained with invasive input function. CBF (ARG) are quantitative CBF values obtained by H_2^{15}O autoradiography, and K_1 and V_d values were calculated from weighted-integration images. Average values for all brain ROIs are plotted.

TABLE 3
Quantitative Analysis Summary

CBV	0.033 ± 0.004 ml/ml
MBF	0.84 ± 0.19 ml/min/g
PTF	0.61 ± 0.09 g/ml
PTI	1.05 ± 0.16
Transit time (LV-to-brain)	2.6 ± 1.4 sec
End-systolic volume of LV	45 ± 14 ml
End-diastolic volume of LV	132 ± 22 ml
Ejection fraction	$66\% \pm 5\%$

CBV = cerebral blood volume; MBF = myocardial blood flow; PTF = perfusable tissue fraction; PTI = perfusable tissue index; LV = left ventricle.

REFERENCES

1. Iida H, Kanno I, Miura S, Murakami M, Takahashi K, Uemura K. Error analysis of a quantitative cerebral blood flow measurement using H_2^{15}O autoradiography and positron emission tomography, with respect to the dispersion of the input function. *J Cereb Blood Flow Metab* 1986;6:536–545.
2. Iida H, Higano S, Tomura N, et al. Evaluation of regional difference of tracer appearance time in cerebral tissues using ^{15}O -water and dynamic positron emission tomography. *J Cereb Blood Flow Metab* 1988;8:285–288.
3. Takikawa S, Dhawan V, Spetsieris P, et al. Noninvasive quantitative fluorodeoxyglucose PET studies with an estimated input function derived from a population-based arterial blood curve. *Radiology* 1993;188:131–136.
4. Eberl S, Anayat AR, Fulton RR, Hooper PK, Fulham MJ. Evaluation of two population-based input functions for quantitative neurologic FDG PET studies. *Eur J Nucl Med* 1997;24:299–304.
5. Iida H, Itoh H, Bloomfield PM, et al. A method to quantitate cerebral blood flow using

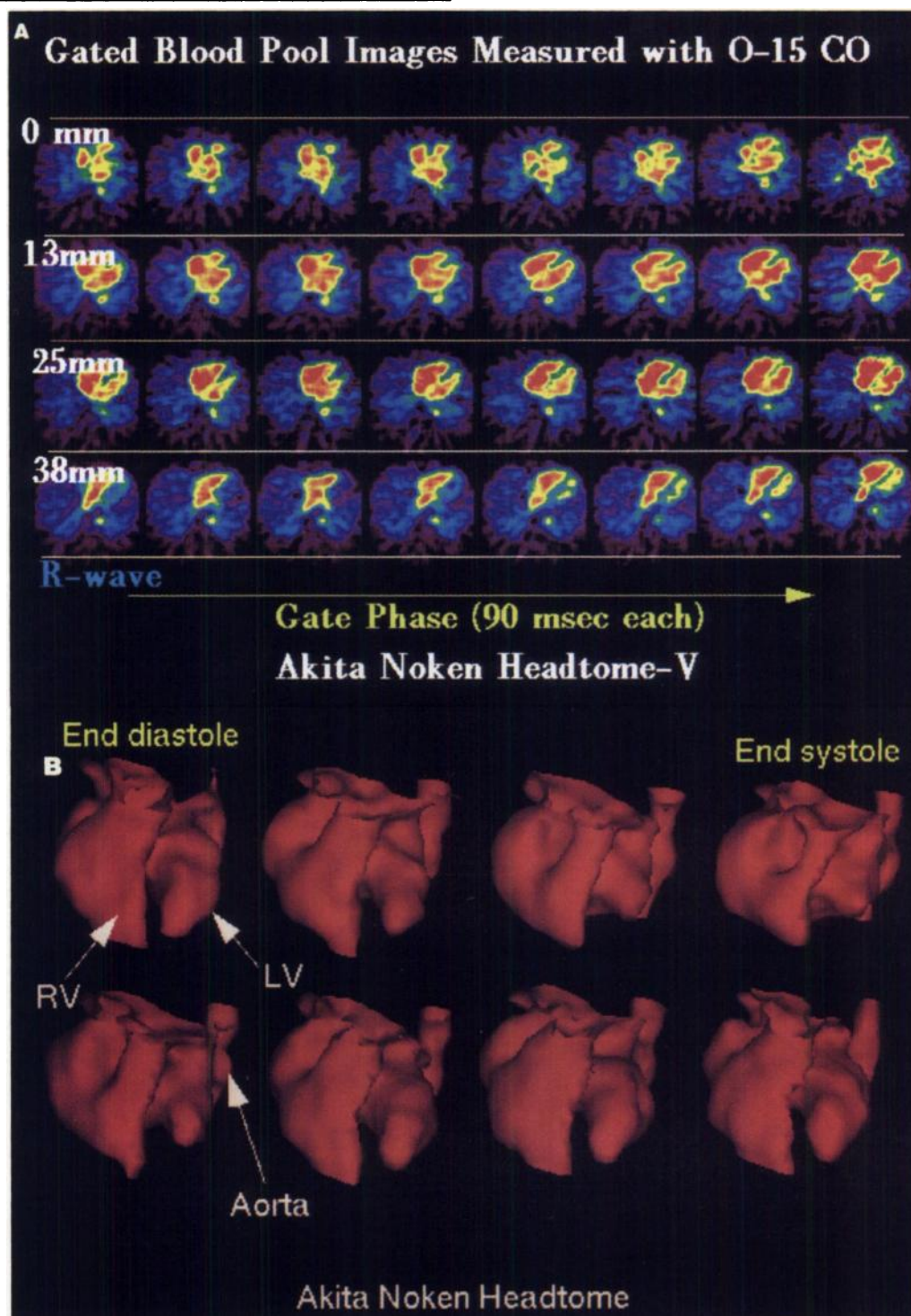


FIGURE 8. Gated blood-pool images (90 msec per frame) obtained from C^{15}O scan. (A) Transaxial images. (B) Surface rendering. Data were acquired for 400 beats. Scan was started 1 min after end of 1 min inhalation of C^{15}O .

- a rotating gamma camera and iodine-123 iodoamphetamine with one blood sampling. *Eur J Nucl Med* 1994;21:1072-1084.
6. Iida H, Itoh H, Nakazawa M, et al. Quantitative mapping of regional cerebral blood flow using iodine-123-IMP and SPECT. *J Nucl Med* 1994;35:2019-2030.
 7. Iida H, Akutsu T, Endo K, et al. A multi-center validation of regional cerebral blood flow quantitation using ^{123}I iodoamphetamine and single photon emission computed tomography. *J Cereb Blood Flow Metab* 1996;16:781-793.
 8. Iida H, Kanno I, Miura S, Murakami M, Takahashi K, Uemura K. A determination of the regional brain/blood partition coefficient of water using dynamic positron emission tomography. *J Cereb Blood Flow Metab* 1989;9:874-885.
 9. Eriksson L, Kanno I. Blood sampling devices and measurements. *Med Prog Tech* 1991;17:249-257.
 10. Kanno I, Iida H, Miura S, Murakami M. Noninvasive measurement of input function by dynamic neck scan for quantitative brain PET using ^{15}O -water [Abstract]. *J Nucl Med* 1991;32(suppl):1003P.
 11. Mejia MA, Itoh M, Watabe H, Fujiwara T, Nakamura T. Simplified nonlinearity correction of oxygen-15-water regional cerebral blood flow images without blood sampling. *J Nucl Med* 1994;35:1870-1877.
 12. Carson RE, Yan Y, Shrager R. Absolute cerebral blood flow with ^{15}O -water. In: Myers R, Cunningham V, Bailey D, Jones T, eds. *Quantitation of brain function using PET*. San Diego, CA: Academic Press; 1996:185-190.
 13. Watabe H, Itoh M, Cunningham V, et al. Noninvasive quantification of rCBF using positron emission tomography. In: Myers R, Cunningham V, Bailey D, Jones T, eds. *Quantitation of brain function using PET*. San Diego, CA: Academic Press; 1996:191-195.
 14. Iida H, Rhodes CG, de Silva R, et al. Use of the left ventricular time-activity curve as a noninvasive input function in dynamic oxygen-15-water positron emission tomography. *J Nucl Med* 1992;33:1669-1677.
 15. Weinberg IS, Huang SC, Hoffman EJ, et al. Validation of PET acquired input functions for cardiac studies. *J Nucl Med* 1988;29:241-247.
 16. Bergmann SR, Herrero P, Markham J, Weinheimer, Walsh MN. Noninvasive quantitation of myocardial blood flow in human subjects with oxygen-15-labeled water and positron emission tomography. *J Am Coll Cardiol* 1989;14:639-652.
 17. Feng D, Li X, Huang SC. A new double modeling approach for dynamic cardiac PET studies using noise and spillover contaminated LV measurements. *IEEE Trans Biomed Eng* 1996;43:319-327.
 18. Iida H, Miura S, Kanno I, Ogawa T, Uemura K. A new PET camera for noninvasive quantitation of physiological functional parametric images: Headtome-V-Dual. In: Myers R, Cunningham V, Bailey D, Jones T, eds. *Quantitation of brain function using PET*. San Diego, CA: Academic Press; 1996:57-61.
 19. Iida H, Bloomfield PM, Miura S, Kanno I, Murakami M, Uemura K. Effect of real-time weighted integration system for rapid calculation of functional images in clinical positron emission tomography. *IEEE Trans Med Image* 1995;14:116-121.
 20. Alpert NM, Eriksson L, Chang JY, et al. Strategy for the measurement of regional cerebral blood flow using short-lived tracers and emission tomography. *J Cereb Blood Flow Metab* 1984;4:28-34.
 21. Raichle ME, Martin WRW, Herscovitch P, et al. Brain blood flow measured with intravenous H_2^{15}O . II. Implementation and validation. *J Nucl Med* 1983;24:790-798.
 22. Kanno I, Iida H, Miura S, et al. A system for cerebral blood flow measurement using an H_2^{15}O autoradiographic method and positron emission tomography. *J Cereb Blood Flow Metab* 1987;7:143-153.
 23. Ardekani BA, Braun M, Hutton BF, Kanno I, Iida H. A fully automatic multimodality image registration algorithm. *J Comp Assist Tomogr* 1995;19:615-623.
 24. Yamaguchi T, Kanno I, Uemura K, et al. Reduction in regional cerebral metabolic rate of oxygen during human aging. *Stroke* 1986;17:1220-1228.
 25. Strother SC, Casey ME, Hoffman EJ. Measuring PET scanner sensitivity: relating count rates to image signal-to-noise ratios using noise equivalent counts. *IEEE Trans Nucl Sci* 1990;37:783-788.
 26. Hatazawa J, Fujita H, Kanno I, et al. Regional cerebral blood flow, blood volume, oxygen extraction fraction, and oxygen utilization rate in normal volunteers measured by the autoradiographic technique and the single breath inhalation method. *Ann Nucl Med* 1995;9:15-21.
 27. Iida H, Kanno I, Takahashi A, et al. Measurement of absolute myocardial blood flow with H_2^{15}O and dynamic positron emission tomography: strategy for quantification in relation to the partial-volume effect. *Circulation* 1988;78:104-115.
 28. Iida H, Rhodes CG, de Silva R, Yamamoto Y, Jones T, Araujo LI. Myocardial tissue fraction: correction for partial volume effects and measure of tissue viability. *J Nucl Med* 1991;32:2169-2175.
 29. Yamamoto Y, De Silva R, Rhodes CG, et al. A new strategy for the assessment of viable myocardium and regional myocardial blood flow using ^{15}O -water and dynamic positron emission tomography. *Circulation* 1992;86:167-178.
 30. de Silva R, Yamamoto Y, Rhodes CG, et al. Preoperative prediction of the outcome of coronary revascularization using positron emission tomography. *Circulation* 1992;86:1738-1742.
 31. Iida H, Rhodes CG, Araujo LI, et al. Non-invasive quantification of regional myocardial metabolic rate of oxygen using $^{15}\text{O}_2$ inhalation and positron emission tomography: theory, error analysis and application in man. *Circulation* 1996;94:808-816.
 32. Yamamoto Y, de Silva R, Rhodes CG, et al. Non-invasive quantification of regional myocardial metabolic rate for oxygen using $^{15}\text{O}_2$ inhalation and positron emission tomography: experimental validation. *Circulation* 1996;94:792-807.
 33. Iida H, Jones T, Miura S. Modeling approach to eliminate the need to separate arterial plasma in oxygen-15 inhalation positron emission tomography. *J Nucl Med* 1993;34:1333-1340.
 34. Iida H, Miura S, Kanno I, Hatazawa J, Ogawa T, Narita Y. Use of a dual-PET system for non-invasive quantitation in O-15 clinical studies [Abstract]. *J Nucl Med* 1996;37(suppl):110P.

Gastric Emptying in Male Neurologic Trauma

Chia-Hung Kao, Sheng-Ping ChangLai, Poon-Ung Chieng and Tzu-Chen Yen

Department of Nuclear Medicine, Taichung Veterans General Hospital, Taichung; Department of Nuclear Medicine, Chung-Shan Medical and Dental College Hospital, Taichung; and Department of Nuclear Medicine, National Taiwan University Hospital and Chang Gung Memorial Hospital, Taipei, Taiwan, Republic of China

Prolonged gastric emptying half-time (GET $_{1/2}$) has been observed in several neurological disorders. Most patients with moderate to severe neurologic trauma (NT) initially do not tolerate enteral or nasogastric feedings. However, previous findings of altered gastric emptying (GE) in patients with NT have been questionable. Quantitative measurements of GE, to determine a possible mechanism for intolerance to enteral feeding, are lacking. In this study, we measured GET $_{1/2}$ sec of solid and liquid meals by radionuclide imaging in men who were neurologic trauma patients. **Methods:** A prospective study was conducted to assess GET $_{1/2}$ in 30 men who were patients with spinal cord injuries (SCIs) and 20 men who were patients with head injuries (HIs) using radionuclide-labeled solid and liquid meals, respectively. Meanwhile, 18 and 14 male control subjects underwent the same imaging techniques for solid and liquid meals, respectively, to evaluate the normal ranges of solid and liquid GET $_{1/2}$ sec (84.5 ± 16.7 and 29.2 ± 3.7 min). **Results:** In the

30 SCI patients, GET $_{1/2}$ of solid meals was significantly prolonged (138.3 ± 49.2 min, $p < 0.05$), and 53% (16/30) of patients had abnormal GET $_{1/2}$. A more prolonged GET $_{1/2}$ and a higher incidence of abnormal GET $_{1/2}$ were observed in patients with high-level injury, when compared with patients with low-level injury ($p < 0.05$). In the 20 HI patients, GET $_{1/2}$ of liquid meals was prolonged significantly (51.7 ± 24.8 min, $p < 0.05$), and 65% (13/20) of patients had abnormal GET $_{1/2}$. Correlation, as indicated by the Glasgow Coma Scale score, was not a statistically significant factor influencing GET $_{1/2}$ ($p > 0.05$). **Conclusion:** NT can cause significantly prolonged GE, especially in patients with high-level SCI.

Key Words: gastric emptying; neurologic trauma; head injury; spinal cord injury

J Nucl Med 1998; 39:1798-1801

In humans, vomiting, abdominal distention and increased gastric residuals after neurologic trauma (NT) suggest the presence of abnormal gastric motility. Despite the clinical significance of abnormal motility, little is known about the gastric effects of NT (1-3). Motility abnormalities might

Received Oct. 14, 1997; revision accepted Jan. 14, 1998.

For correspondence or reprints contact: Chia-Hung Kao, MD, Department of Nuclear Medicine, Taichung Veterans General Hospital, 160 Taichung Harbor Road, Section 3, Taichung 40705, Taiwan, Republic of China.



The Journal of
NUCLEAR MEDICINE

Noninvasive Quantitation of Cerebral Blood Flow Using Oxygen-15-Water and a Dual-PET System

Hidehiro Iida, Shuichi Miura, Yasuaki Shoji, Toshihide Ogawa, Hirotsugu Kado, Yuichiro Narita, Jun Hatazawa, Stefan Eberl, Iwao Kanno and Kazuo Uemura

J Nucl Med. 1998;39:1789-1798.

This article and updated information are available at:

<http://jnm.snmjournals.org/content/39/10/1789>

Information about reproducing figures, tables, or other portions of this article can be found online at:


<http://jnm.snmjournals.org/site/misc/permission.xhtml>

Information about subscriptions to JNM can be found at:

<http://jnm.snmjournals.org/site/subscriptions/online.xhtml>

The Journal of Nuclear Medicine is published monthly.
SNMMI | Society of Nuclear Medicine and Molecular Imaging
1850 Samuel Morse Drive, Reston, VA 20190.
(Print ISSN: 0161-5505, Online ISSN: 2159-662X)

© Copyright 1998 SNMMI; all rights reserved.

 SOCIETY OF
NUCLEAR MEDICINE
AND MOLECULAR IMAGING